



# A Nanoscale Modification of Materials at Thermoplasmonic Laser-Induced Backside Wet Etching of Sapphire

O. M. Zhigalina<sup>1,2</sup> · D. N. Khmelenin<sup>1</sup> · A. V. Atanova<sup>1</sup> · N. V. Minaev<sup>1</sup> · A. P. Sviridov<sup>1</sup> · M. Yu. Tsvetkov<sup>1</sup>

Received: 30 July 2019 / Accepted: 11 November 2019 / Published online: 27 November 2019  
© Springer Science+Business Media, LLC, part of Springer Nature 2019

## Abstract

Laser-induced backside wet etching using water solution of plasmon precursor ( $\text{AgNO}_3$ ) as an absorbing medium provides effective structuring of such a complex material as sapphire. At the same time, this process is accompanied by the formation of silver nanoparticles and a significant modification of a surface layer of sapphire. Hybrid plasmon structures are formed on the surface of sapphire. In this paper, the structure and phase composition of surface layer formed during the transformation of the materials in the process of etching have been studied using electron microscopy methods, electron diffraction, and EDX analysis; possibilities of creating of new plasmon nanostructures have been analyzed.

**Keywords** Laser-induced backside wet etching (LIBWE) · Plasmonics · Microstructuring · Nanoparticles · Electron microscopy · EDX analysis

## Introduction

Significant progress in the creation of new functional materials was achieved in experiments on the interaction of laser radiation with the materials. This is determined mainly by the use of ultrashort pulse lasers and high-intensity radiation sources. Many works are dedicated to obtaining and modification of various nanoparticles (see, e.g., [1–5]). Experiments on laser ablation allowed establishing that femtosecond laser exposure induces phase transformations on the sample surface that change the medium structure [6, 7]. At the same time, such experiments are usually carried out using unique devices and require serious resources.

In 1999, during studies of laser microstructuring, a method of indirect impact of laser radiation on the materials was proposed [8, 9]. In this process, high-intensity laser radiation focuses on the back surface of a transparent dielectric, which is located in a cell filled with highly absorbing liquid. A series of processes occur in the field of focus, on the sample/liquid interface: nonlinear absorption; absorption on defects;

photochemical, thermal, and hydrodynamic processes; the formation of a supercritical fluids; cavitation; melting; evaporation; etc. [10–12]. These processes lead to the formation of a substantially localized area with extremely high temperature and pressure on a liquid/solid interface, and the accompanying strong pressure gradients at the same time contribute to the removal of the matter from the treatment area.

The developed version of this technology was called laser-induced backside wet etching (LIBWE) [13]. This technology requires highly absorbent organic liquids or solutions as an absorbent medium. Subsequently, it has been proposed to use inorganic fluids, metals, both liquid and solid, solid-state absorbers, laser plasma, and artificially formed absorbent layers as absorbent media.

This paper examines the results of this approach, where a solution of plasmon precursor is used to create an absorbent medium. The implementable version of thermoplasmonic LIBWE (TP-LIBWE) [14, 15] provides etching of such difficult-to-process material as sapphire (as well as other promising optical materials such as glass, quartz, diamond). At the same time, the process provides, in comparison with other LIBWE technologies, record etching speeds reaching several microns per pulse at energy densities  $\leq 12 \text{ J/cm}^2$  [15].

During this process, various phase transformations occur in the surface layer of sapphire; there is also significant modification of the materials, which is usually achieved only with femtosecond laser impacts (see, e.g., [6]). In addition, as a result of interaction with plasmon precursor, a silver nanolayer

✉ M. Yu. Tsvetkov  
mtsvet52@mail.ru

<sup>1</sup> Federal Scientific Research Centre “Crystallography and Photonics”, Russian Academy of Sciences, Moscow 119333, Russia

<sup>2</sup> Bauman Moscow State Technical University, Moscow 105005, Russia

is formed, which allows considering the obtained structures in the context of the perspective of potential plasmonic applications. In this paper, the structure and phase composition of the obtained plasmon nanostructures have been studied using optical, scanning electron (SEM), transmission electron microscopy (TEM), as well as high-resolution electron microscopy (HREM), energy-dispersive X-ray spectroscopy (EDX microanalysis), and EDX-mapping. Changes of the substance and possible use of the obtained materials are discussed.

## Experiment and Diagnostics

### Laser Experiment and Materials

The concept of laser experiment and the corresponding setup is described in the works [16, 17] dedicated to the various modes of optical glass etching.

Sapphire substrates in base orientation with a diameter of 50.8 mm and a thickness of  $\sim 0.45$  mm were polished on both sides for optical investigations. The substrates were obtained from sapphire monocrystals grown through the Kirpoulos-Musatov method [18]. Samples were irradiated with a solid-state diode-pumped laser TECH-527 Basic (Laser compact, Russia) with the wavelength  $\lambda = 527$  nm, duration of the laser pulse  $\tau = 5$  ns, and maximum pulse energy  $E = 250$   $\mu$ J. The etched plate was installed as a front wall of a demountable cell filled with working liquid—saturated 5-molar silver nitrate ( $\text{AgNO}_3$ ) water solution, laser-induced decomposition of which provides highly absorbing silver nanoparticles (npAg), and a thermoplasmonic effect in the system.

Experiments on laser plasmon microstructuring of sapphire samples were conducted at a pulse frequency of 1 kHz and laser radiation energies up to 25  $\mu$ J per pulse. The sample was irradiated with focused (the back plane of the plate in the area of laser beam waist) and unfocused beams (beam waist was shifted into absorbing liquid at distances up to 20  $\mu$ m). This allowed forming areas with the following parameters in the area of focus on the interface between the sample and absorbent liquid: the diameter of laser beam waist from 3.4 to 9.6  $\mu$ m (at  $1/e$  level) and depth of focus from  $\sim 30$  to  $\sim 300$   $\mu$ m. When the focus shifted, the diameter of the beam in the etching area increased up to 20  $\mu$ m. The energy density for the discussed conditions reached  $\Phi \approx 30$  J/cm<sup>2</sup>. Channels were formed at a laser beam scanning rate from 8 to 140  $\mu$ m/s.

### Structures, Sample Preparation, and Electron Microscopy Techniques

The geometry, shape, and structural state of the sample surface were studied using optical, scanning electron, and transmission electron microscopy. Optical microscopic images of laser structures at different densities of the energy of laser pulses

were obtained using an optical microscope HRM-300 (Huvitz, Korea) with 3D imaging of surface topography (see [15]). SEM images were obtained in a FEI Scios microscope at accelerating voltage  $U = 2$  kV in the secondary electron mode using the Everhart-Thornley detector.

Figure 1 presents SEM images of a sapphire plate with channels obtained through LIBWE structuring. Channels of different depths from 12  $\mu$ m to 220  $\mu$ m are clearly visible in Fig. 1a.

This work contains more detailed studies of the oblique channel and its surroundings, where several types of formed nanostructures were registered. The channel is characterized by oblique walls and has a depth of 6.5  $\mu$ m and a horizontal width of 4.7  $\mu$ m in the middle of depth; its enlarged image is shown in Fig. 1b.

The structure of the sapphire surface in the channel was investigated with transmission electron microscopy, high-resolution electron microscopy, scanning transmission electron microscopy with high-angle annular dark field detector (HAADF STEM), electron diffraction, energy-dispersive X-ray analysis, and EDX-mapping in a FEI Tecnai Osiris microscope with an accelerating voltage of 200 kV. EDX analysis and elemental mapping were performed in a special SuperX EDS system with four silicon detectors. The system is designed for rapid obtaining (for several minutes) large area maps of chemical element distribution. Electron microscopy images were processed and analyzed using Digital Micrograph, Esprit, TIA, and JEMS software (see, e.g., [19]).

The cross section of this channel made with a focused ion beam (FIB) in a FEI Scios double beam system has been investigated using TEM methods. To prepare the cross-section sample, two technological layers were applied; they are visible in Fig. 2: a layer of copper deposited on the surface of sapphire plate in order to drain the charge from the nonconductive sample during SEM studies and a layer of platinum locally applied in order to protect the channel surface from ion etching during the FIB preparation of a lamella for TEM studies. These technological layers are clearly visible in the channel cavity in Fig. 2.

## Experimental Results

### Processes on Sapphire Surface

Figure 2 shows a HAADF STEM image of the channel cross section and its elemental map. The HAADF STEM image describes the relief that is formed on channel walls after exposure to laser radiation. Inner walls of the sapphire channel that are outlined in blue on the elemental maps possess clearly visible heterogeneous relief. They are more clearly expressed on the left wall, which was slanted toward the laser beam, while the right wall hung over the groove (Fig. 1b). The

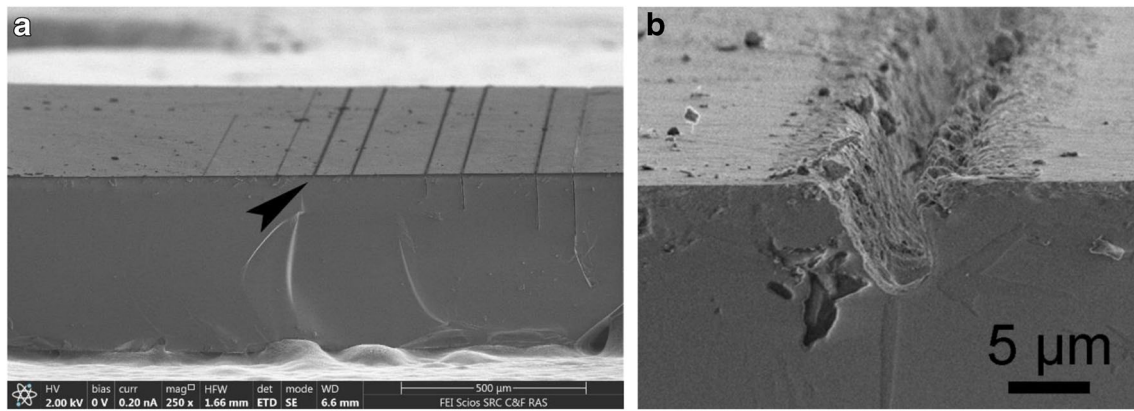


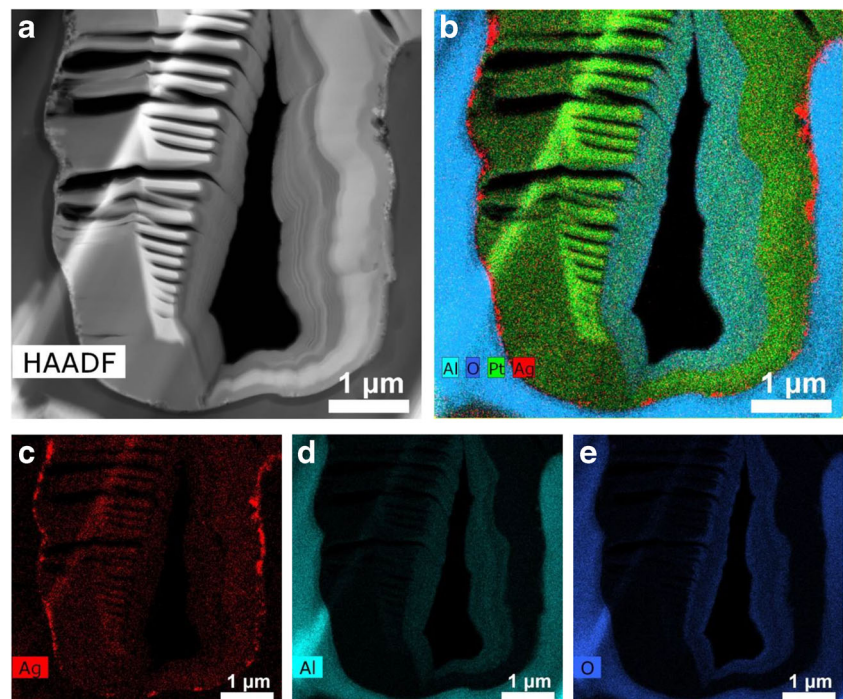
**Fig. 1** SEM images of sapphire with channels obtained using LIBWE: **(a)** general view of the plate with channels; **(b)** magnified image of the oblique channel (marked in Fig. 1a with a black arrow)

presence of the relief can be explained by the fact that the channel was formed in the “strong” etching (ablation) mode (see [15]). The HAADF STEM image shows a darker layer along the entire channel surface. The layer repeats the heterogeneous relief of the channel walls. It is almost continuous and has a thickness of up to 170 nm. At the same time, its thickness is greater on the left side of the channel and clearly thinner on the right overhanging side. The channel cavity, its central part, is filled not only with platinum and copper but also with spraying products formed during manufacturing and thinning of the lamella with a focused ion beam. An enlarged HAAADF STEM image of the surface area is shown in Fig. 3a. The thickness of the dark layer in this region reaches 170 nm. A thin discontinuous layer of silver is observed on the surface of the dark layer (sapphire) (Fig. 2b, c, 3).

Changing of element concentrations in the sapphire—dark layer—silver area is shown in Fig. 3b. Normalized concentration profiles obtained along the vertical yellow line drawn in Fig. 3a are virtually unchanged in the sapphire area. This fact indicates that no other elements have been found in the dark layer except of Al and O. In this regard, taking into account  $z$ -contrast STEM image formation, one can assume that the dark contrast is caused only by the presence of the less dense amorphous layer.

A more detailed interface structure in the dark layer area has been studied by TEM methods. Figure 4 shows an image of the sapphire—silver interface area, where this layer looks light gray due to the peculiarity of contrast formation in the bright field (BF) TEM mode. It is marked as “am- $\text{Al}_2\text{O}_3$ .” A selected area electron diffraction (SAED) pattern (Fig. 4b)

**Fig. 2** General view of the channel with an amorphous layer and silver nanoparticles: HAADF STEM image **(a)** and corresponding elemental maps **(b–e)**



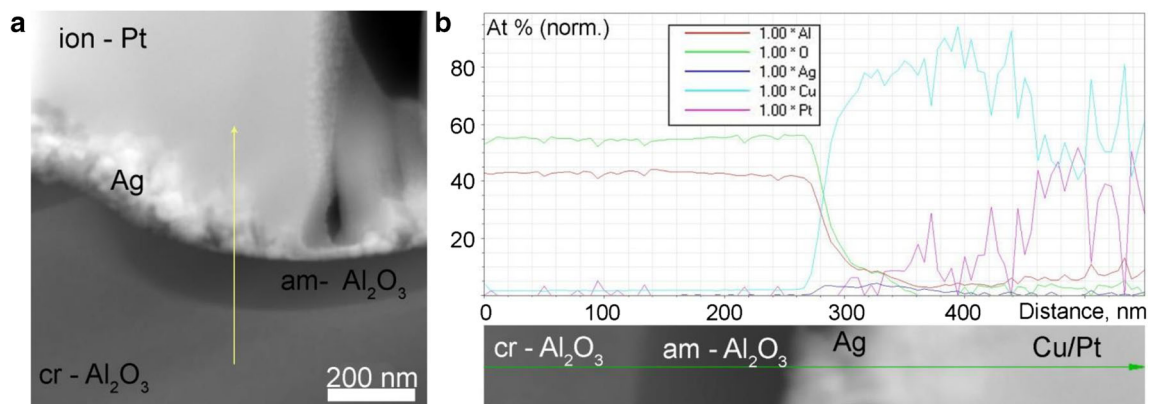


**Fig. 3** HAADF STEM image (a) and concentration profiles of chemical element distribution measured along the vertical yellow line (b). am- $\text{Al}_2\text{O}_3$  is a layer of amorphized sapphire, cr- $\text{Al}_2\text{O}_3$  is a layer of crystalline sapphire, and ion-Pt is a technological layer of Pt and Cu

clearly shows single crystalline sapphire reflections (the layer is marked as “cr- $\text{Al}_2\text{O}_3$ ”) with the  $[1\bar{1}0]$  zone axis. Some reflections in the SAED pattern correspond to the interplanar distances of silver with the *fcc* unit cell. The silver layer is darker by contrast in the BF TEM image. HREM images of the am- $\text{Al}_2\text{O}_3$  layer have proved that it has no crystalline structure, i.e., it is amorphous.

A study of the behavior of the amorphous layer under the electron beam has shown that it is unstable and crystallizes with the formation of the same phase as cr- $\text{Al}_2\text{O}_3$  substrate. Figure 5 illustrates the crystallization process of the amorphous layer under the electron beam, which occurs in a few seconds. Fourier diffractograms in Fig. 5a were taken from the cr- $\text{Al}_2\text{O}_3$  layer and in Fig. 5b—from newly appeared crystals; they are identical to the electron diffraction pattern from crystalline sapphire shown in Fig. 3b. Comparison of Fig. 5a and 5b clearly shows that the amorphous am- $\text{Al}_2\text{O}_3$  layer has become much thinner due to the newly grown crystals of the sapphire substrate. Thus, in this case, growth of sapphire crystals under the electron beam occurred from the sapphire—amorphous layer interface and was heterogeneous. Black arrows in Fig. 5b mark the boundaries of newly grown oriented crystals. Figure 6 shows that growth of sapphire crystals under the electron beam in the amorphous layer can start also in the

volume of the layer itself, i.e., be homogeneous, with the formation of randomly oriented small crystals.

TEM studies of the silver layer structure have shown that silver nanoparticles are mainly localized on the upper surface of the amorphous layer or in its top area (Fig. 3a). The size of particles varies in a wide range—from 1–2 to 60 nm. The SAED pattern (Fig. 4b) demonstrates rings corresponding to polycrystalline silver. Weak reflections of polycrystalline copper are also seen in the microdiffraction pattern due to the presence of the abovementioned deposited technological layer.

### Hybrid Plasmon Structures

Several clusters of silver nanoparticles were found on walls at the entrance of the oblique channel. Figure 7 presents a HAADF STEM image and elemental maps in this area. A study of the distribution of chemical elements in the cluster under a higher magnification in the electron microscope (Fig. 8) has illustrated that silver nanoparticles are placed in the aluminum-oxygen matrix and are therefore tightly fixed on the surface of the channel. The size of the largest silver particles in this cluster reaches 60 nm.

**Fig. 4** TEM image of the interface sapphire, silver (a), and corresponding SAED pattern (b). Black numbers indicate reflections corresponding to the crystalline sapphire substrate; red circles mark rings corresponding to planes (111), (200), and (220) of silver with *fcc* lattice

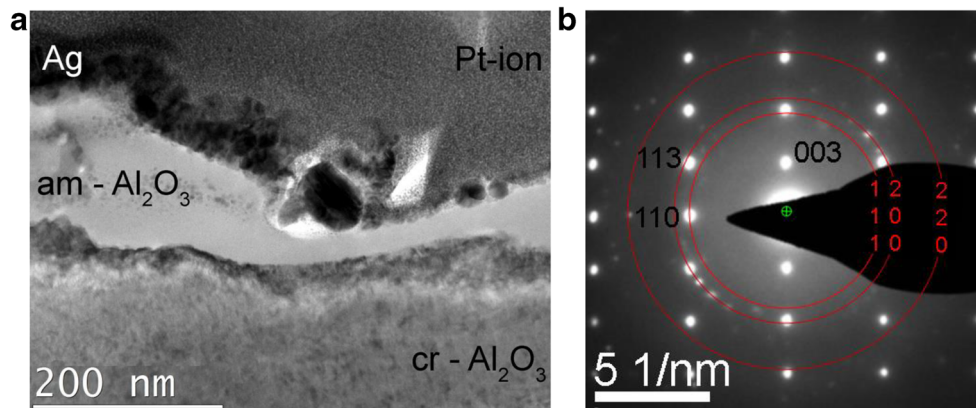
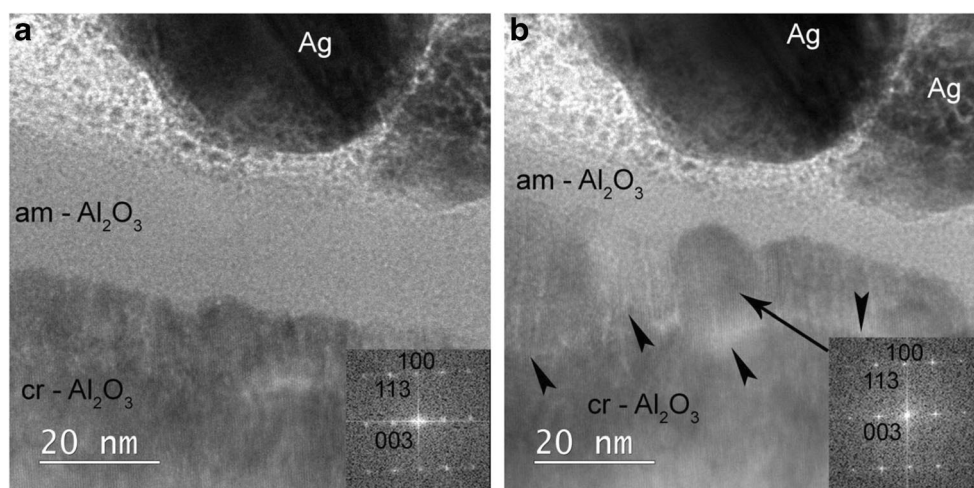


**Fig. 5** Crystallization of the amorphous layer under the electron beam on the interface silver-sapphire: a BF TEM image of the interface sapphire/amorphous layer and the corresponding Fourier diffractogram at the beginning (a) and at the end of observation (b). Black arrows indicate the border of newly grown oriented crystals



A more detailed analysis of the structural state was carried out using TEM methods. Figure 9 presents BF and dark field (DF) TEM images and the corresponding microdiffraction pattern of this cluster. According to these images, the nanoparticles demonstrate an arbitrary shape. The particle size varies mainly in the range of  $23.2 \pm 11.55$  nm. The ring electron diffraction pattern is typical for fine-grained polycrystalline materials (Fig. 9c). It is evident that the location of rings is typical for metals with the *fcc* unit cell. The set of interplanar distances  $d_{hkl}$  corresponds to silver. The first ring (corresponding interplanar distance  $d = 3.03$  Å), as well as individual reflections that are not located on the main rings of the SAED pattern and are indicated by arrows, refers to compounds such as  $\text{AgNO}_x$  ( $x = 2-3$ ) according to electron diffraction pattern calculations.

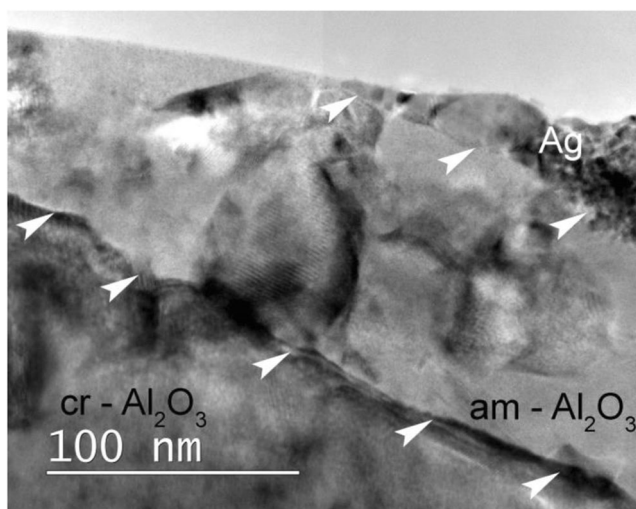


**Fig. 6** Crystallization of the amorphous layer under the electron beam on the interface silver-sapphire: a BF TEM image of the amorphous layer with the formation of randomly oriented sapphire crystals. White arrows indicate the upper and lower boundaries of the layer

Images of individual particles of different sizes from the studied cluster obtained by HREM are presented in Figs. 10 and 11. As can be seen from TEM and HREM images, there are characteristic stripes in many nanocrystals, which indicate the presence of twins, i.e., formed nanoparticles are characterized by a high concentration of defects. At the same time, it can be observed multiple twinning in the images of such nanoparticles [20–22], which allows them to have different external shape (habitus) and structure. Figure 10a shows an image of such kind of particle. Filtered HREM images and the Fourier diffractograms taken from various areas have shown that it is Ag particle with the *fcc* lattice, the cell parameters of which are no different from the ones for bulk materials; its size reaches 25 nm. Straight white lines on the enlarged filtered area (Fig. 10b) indicate projections of twinning planes. Inverse Fourier transform makes it possible to clearly observe twins in the nanoparticle's structure. As usual for crystals with the *fcc* lattice, they are located in  $\{111\}$  crystallographic planes.

One can see from the HREM image in Fig. 11a that the aluminum-oxygen matrix enveloping silver particles is amorphous. The formed cluster appears as a drop of sapphire that captured silver nanoparticles during cooling process. The Fourier analysis of HREM images of particles has revealed interplanar distances  $d = 2.28$  Å, 2.17 Å, and 2.03 Å. These distances are shown in particle images in Fig. 11b. The first two of the values significantly differ from those for silver ( $d = 2.359$  Å; 2.044 Å). Given the accuracy of TEM measurements, these distances can be attributed to both the  $\text{AgNO}_3$  phase and  $\delta\text{-Al}_2\text{O}_3$  phase.

## Discussion and Perspective

When using hydrocarbon liquids as an absorbent medium, the advantages of LIBWE technology were clearly revealed [13,

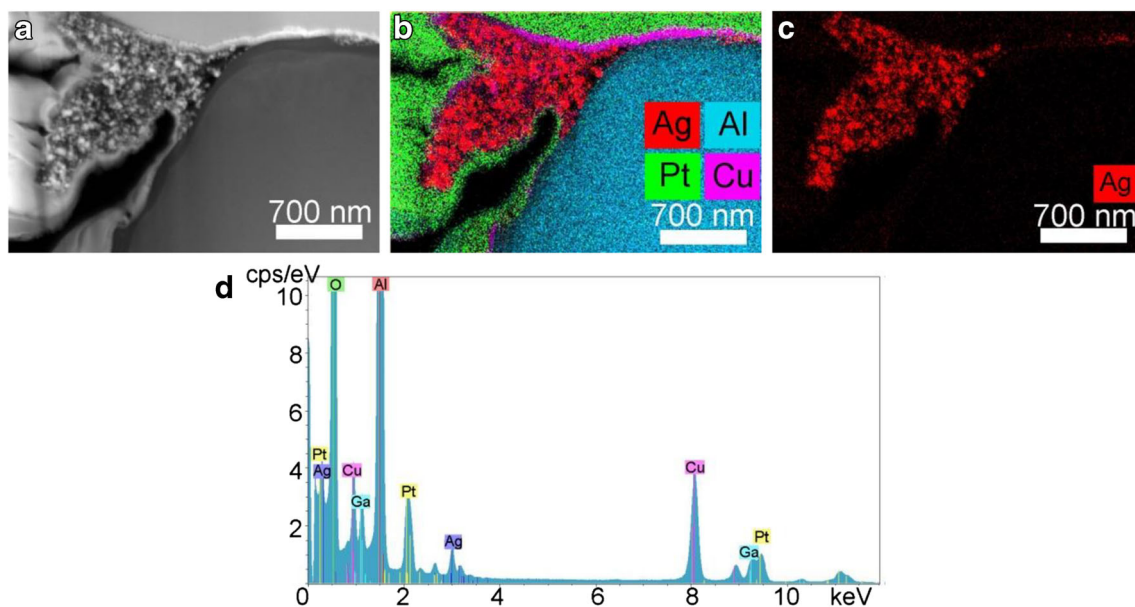


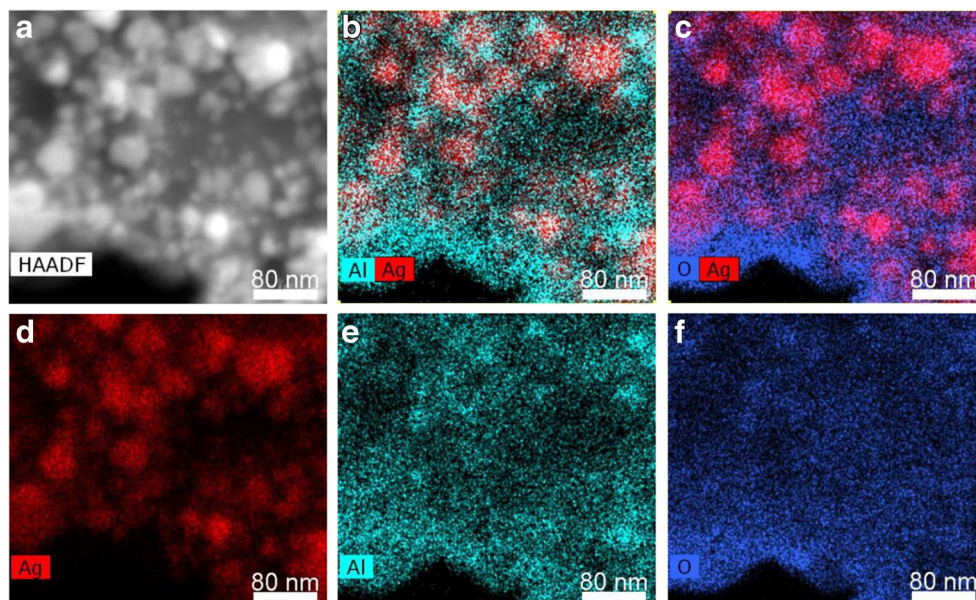
**Fig. 7** HAADF STEM image of the Ag nanoparticle cluster at the channel entrance (a), elemental maps (b, c), and the corresponding EDX spectrum (d)

23, 24]. In this case, exposure to laser radiation causes the decomposition of the organic medium with the formation of a highly absorbing layer of carbon. The confinement mode is implemented, when laser radiation is almost completely absorbed in the highly localized area between the sample and the carbon layer. Such a mode contributes to the “enhancement” of processes that occur when laser radiation interacts with the materials and allows to create conditions close to those realized in the case of femtosecond pulses.

Further progress in this direction can be achieved applying thermoplasmonic LIBWE (see diagram in Fig. 12a). The intensive laser irradiation of silver nitrate water solution triggers

a mechanism of precursor reduction to silver nanoparticles. Laser radiation initiates the formation of active intermediates in the solution, which leads to the formation of  $\text{Ag}^0$  silver atoms [25, 26] with a gradual transition from individual atoms to nanoparticles and clusters of silver [27, 28]. At the same time, the first “seed” pulses of laser radiation form centers of additional “plasmonic” absorption; the process develops avalanche-like. In the interface of the treated sample surface, an area with a high concentration of plasmon nanoparticles with a maximum plasmonic absorption near  $\lambda \approx 430$  nm and a wide long wavelength wing (see Fig. 5c in work [14]) is formed. This indicates the appearance of spherical and quasi-spherical

**Fig. 8** HAADF STEM image (a) and elemental maps of the Ag nanoparticles formed on the channel wall (b–f)



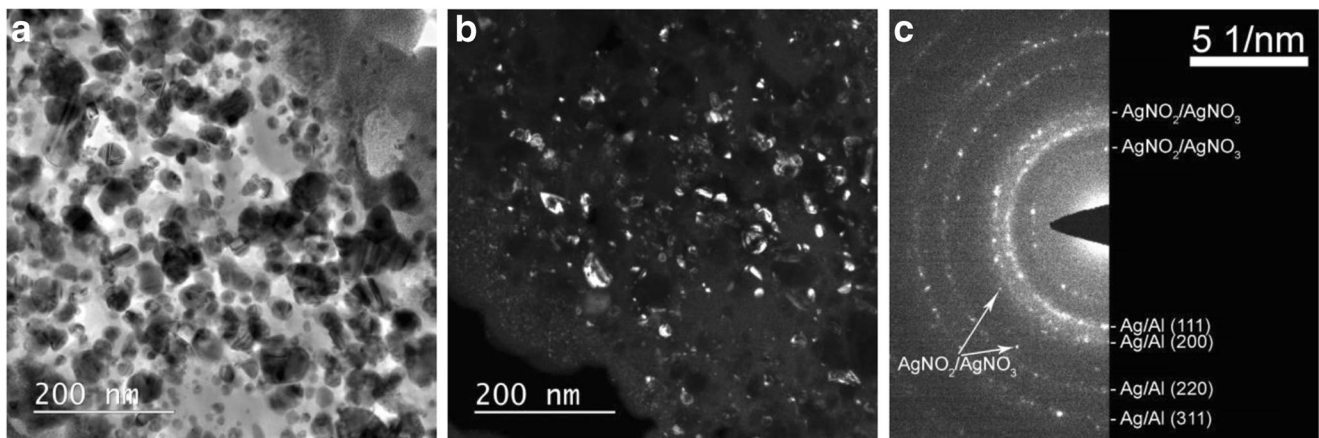


**Fig. 9** BF (a) and DF (b) TEM images of silver particles and the corresponding SAED pattern (c)

silver nanoparticles with significant spread in size in the working fluid [29]. Such “plasmon cloud” provides extremely high absorption of laser radiation on the sapphire surface.

The achieved temperatures and pressures (temperatures can reach several thousand of Kelvins and pressures can be several gigapascals [1]) provide superfast heating of the solution and dielectric to extremely high temperatures and the transition of the substance into the supercritical state. In a time range of  $10^{-10}$  -  $10^{-7}$  s, “plasma plume” is formed that facilitates a removal of the materials out of the etching area [3]. After the laser pulse, the pressure and temperature of the medium begin to decrease, the processes of nucleation and formation of nanoparticles and nanoclusters occur in the precursor solution, and a significantly modified layer is formed on the sapphire surface (see Fig. 12b).

The structure of the core-shell nanoparticles, obtained through laser ablation, was discussed in the articles [30–32]. However, unlike the nano-objects obtained in this work, in [30], Ag nanoparticles are covered with several nanometer-thick  $\text{Al}_2\text{O}_3$  shells. The morphology and size of the particles directly affect their plasmon resonance optical properties [33,

34]. The control of optical properties of silver nanoparticles by varying of technological parameters and subsequent of thermal treatment makes them highly promising for the development of optical microscopy and biological research [33].

Aluminum oxide ( $\text{Al}_2\text{O}_3$ ) can exist in several polymorphic forms: out of which, the most thermodynamically stable one under the standard conditions is  $\alpha$ - $\text{Al}_2\text{O}_3$  (corundum) [35]. At the same time, with external influence (temperature, pressure), aluminum oxide can turn into other crystalline, for example,  $\gamma$ - $\text{Al}_2\text{O}_3$ , or amorphous phases [6, 36]. In our case, thermoplasmonic LIBWE leads to the formation of an amorphous aluminum-oxygen matrix with embedded silver nanoparticles on the sapphire surface. Such polymorphic transitions are of significant interest in terms of studying the structure of the materials.

The development of laser technology allowed to discover that ultrashort laser pulses enable the transition of sapphire into amorphous phase, which can be easily treated by conventional liquid etching. A number of works report a similar two-stage process [37–39]. When using nanosecond pulses, laser radiation is absorbed by hot carriers (electrons) that heat

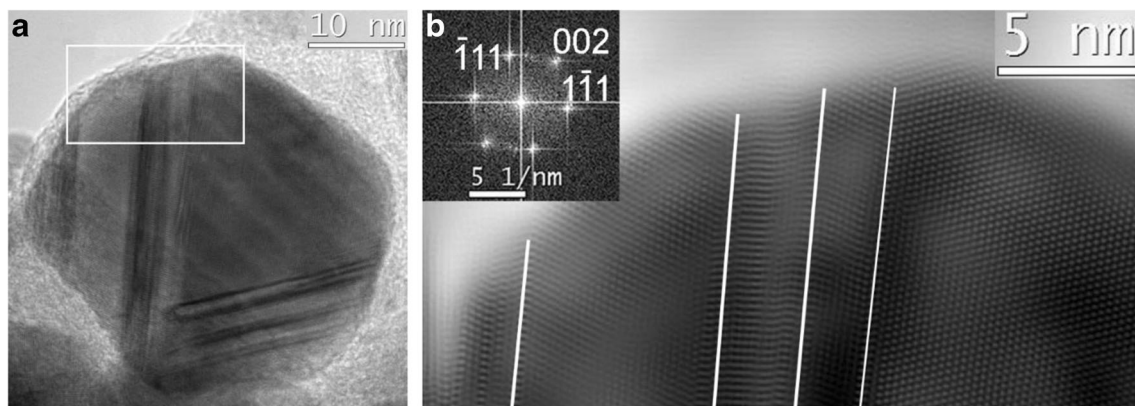


**Fig. 10** HREM images of a large Ag particle: (a) general view; (b) enlarged filtered HREM image of the particle area highlighted by a white rectangle. White lines indicate twinning  $\{111\}$  planes; (inset) Fourier diffractogram taken from the particle area, the  $[110]$  zone axis

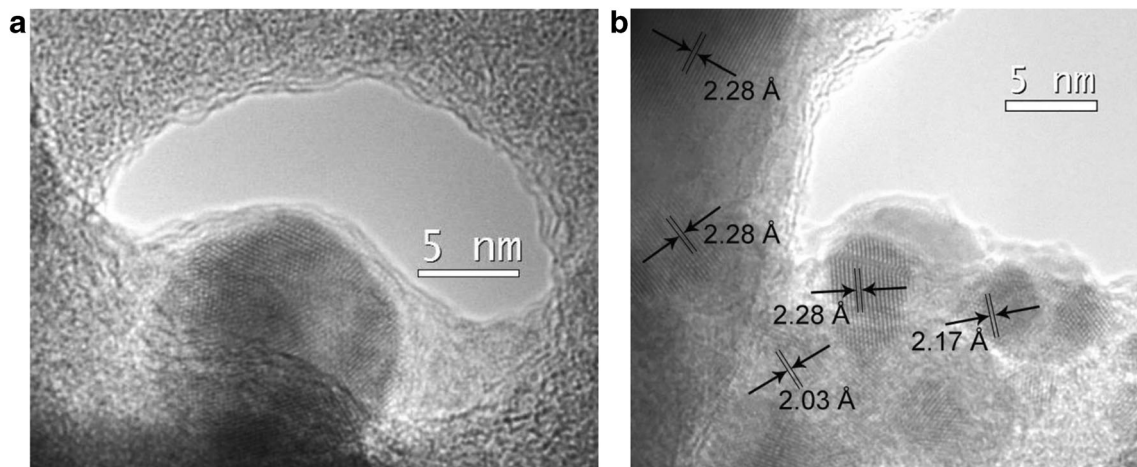


**Fig. 11** HREM images of the Ag nanoparticle in the amorphous matrix (a) and particles of different sizes with interplanar distances that are different from  $d$  for silver (b)

initially cold ions with reaching equilibrium time in the range of  $\tau_E \sim 10^{-12}$ – $10^{-11}$  s [40]. After the heating process, a balance is established between electrons and phonons, and phase changes can be considered as a thermal process with quasi-equilibrium thermodynamic states involving the entire volume of the materials. In the process of thermoplasmonic LIBWE, achieved temperatures and pressures provide extremely high etching speeds [15].

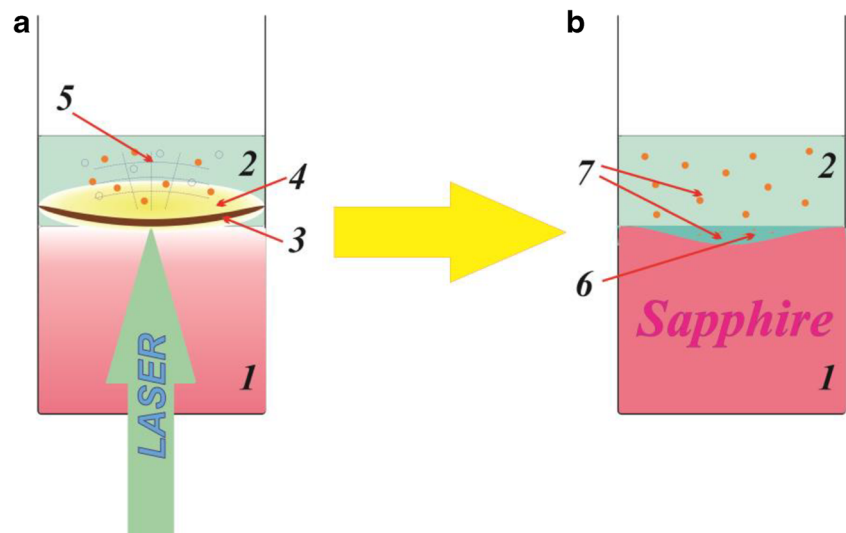
The developed technological process can be very interesting in terms of creating a component base for different areas of plasmonics. The silver nanolayer formed during this process can be used for manufacturing of the analogs of channel [41] and/or chain [42] plasmonic waveguides, as well as for the structures for plasmonic microfluidics [43]. In addition, such plasmonic structures can become a basis for the creation of different types of plasmonic sensors [44], e.g., SERS sensors.

## Conclusion

In this work, microstructuring of such high-demand material as sapphire was carried out using thermoplasmonic laser-induced backside wet etching (TP-LIBWE). Electron microscopy and EDX mapping methods were used for studying the channels and hybrid plasmonic structures formed on the sapphire surface as a result of laser thermoplasmonic impact.

It was established that under the influence of laser radiation, plasmonic precursor ( $\text{AgNO}_3$ ) is reduced to silver nanoparticles, which provide huge absorption of laser radiation. Due to this, a substantially localized area with extremely high temperatures and pressures providing sapphire ablation was formed in the absorbing solution—sample interface. It was shown that in this case, significant phase changes of the substance occurred: the amorphous phase with embedded silver

**Fig. 12** Diagram for the implementation of thermoplasmonic LIBWE (a) and the resulting formation of nanomaterials (b) 1 sapphire plate; 2 plasmonic precursor; 3 “plasmonic absorbent cloud;” 4 plasma plume; 5 spreading shock waves, flying bubbles, and nanoparticles; 6 amorphous modified sapphire layer; 7 nanoparticles





nanoparticles was formed on the surface of the crystalline sapphire. The thickness of the surface amorphous sapphire layer was up to 170 nm. Its crystallization was activated by an electron beam in a transmission electron microscope. The thickness of the layer with silver nanoparticles reached 50 nm; the size of nanoparticles varied in the range of 2–60 nm. The nanoparticles were located both in the amorphous layer and on its surface. It was established that the presence of twins was a characteristic feature of the nanoparticles observed. The structural changes initialized by TP-LIBWE, and possible applications of the formed structures were discussed.

**Acknowledgments** This work was supported by the Ministry of Science and Higher Education within the State assignment FSRC «Crystallography and Photonics» RAS in part of the TEM and SEM investigation and development of microstructuring technologies and the Russian Foundation for Basic Research in part of the design of the laser facility (Grant No. 18-02-00420 A) and in part of the studies on sapphire etching processes (Grant No. 18-29-06056 MK). Electron microscopy investigations were carried out using equipment of the Shared Research Center of the Institute of Crystallography, Russian Academy of Sciences (project RFMEFI62119X0035).

## References

- Yang GW (2007) Laser ablation in liquids: applications in the synthesis of nanocrystals. *Prog Mater Sci* 52:648–698
- Yan Z, Chrisey DB (2012) Pulsed laser ablation in liquids for micro-/nanoscale generation. *J Photochem Photobiol C: Photochem Rev* 13:204–223
- Amendola V, Meneghetti M (2013) What controls the composition and the structure of nanomaterials generated by laser ablation in liquid solution? *Phys Chem Chem Phys* 15:3027–3046
- Makarov GN (2013) Laser applications in nanotechnology: nanofabrication using laser ablation and laser nanolithography. *Phys Usp* 56:643–682
- Ionin AA, Kudryashov SI, Samokhin AA (2017) Material surface ablation produced by ultrashort laser pulses. *Phys Usp* 60:149–160
- Juodkazis S, Nishimura K, Misawa H, Ebisui T, Waki R, Matsuo S, Okada T (2006) Control over the crystalline state of sapphire. *Adv Mater* 18:1361–1364
- Vailionis A, Gamaly EG, Mizeikis V, Yang W, Rode AV, Juodkazis S (2011) Evidence of superdense aluminium synthesized by ultrafast microexplosion. *Nat Commun* 2:445
- Wang J, Niino H, Yabe A (1999) One-step microfabrication of fused silica by laser ablation of an organic solution. *Appl Phys A* 68:111–113
- Wang J, Niino H, Yabe A (1999) Micromachining of quartz crystal with excimer lasers by laser-induced backside wet etching. *Appl Phys A* 69:S271–S273
- Niino H, Yasui Y, Ding X, Narazaki A, Sato T, Kawaguchi Y, Yabe A (2003) Surface micro-fabrication of silica glass by excimer laser irradiation of organic solvent. *J Photochem Photobiol A: Chem* 158:179–182
- Vass C, Budai J, Schay Z, Hopp B (2010) Interpretation and modeling of laser-induced backside wet etching procedure. *J Laser Micro/Nanoeng* 5:43–47
- Zimmer K, Böhme R, Ehrhardt M, Rauschenbach B (2010) Mechanism of backside etching of transparent materials with nanosecond UV-lasers. *Appl Phys A* 101:405–410
- Zimmer K, Ehrhardt M, Böhme R (2012) Laser-induced backside wet etching: processes, results, and applications. In: Yang G (ed) *Laser ablation in liquids: principles and applications in the preparation of nanomaterials*. Pan Stanford Publishing, Singapore, pp 1013–1123
- Tsvetkov MY, Yusupov VI, Minaev NV, Timashev PS, Golant KM, Bagratashvili VN (2016) Effects of thermo-plasmonics on laser-induced backside wet etching of silicate glass. *Laser Phys Lett* 13:106001
- Tsvetkov MY, Minaev NV, Akovantseva AA, Timashev PS, Muslimov AE, Kanevskii VM (2019) Thermoplasmonic laser-induced backside wet etching of sapphire. *Quantum Electron* 49:133–140
- Tsvetkov MY, Yusupov VI, Minaev NV, Akovantseva AA, Timashev PS, Golant KM, Chichkov BN, Bagratashvili VN (2017) On the mechanisms of single-pulse laser-induced backside wet etching. *Opt Laser Technol* 88:17
- Tsvetkov MY, Yusupov VI, Timashev PS, Golant KM, Minaev NV, Tsykina SI, Bagratashvili VN (2017) On the role of supercritical water in laser-induced backside wet etching of glass. *Russ J Phys Chem B* 11:1061–1069
- Muslimov AE, Asadchikov VE, Butashin AV, Vlasov VP, Deryabin AN, Roshchin BS, Sulyanov SN, Kanevsky VM (2016) Supersmooth and modified surface of sapphire crystals: Formation, characterization, and applications in nanotechnologies. *Cryst Rep* 61:730–743
- <https://www.gatan.com>
- Wang ZL (2000) Transmission electron microscopy of shape-controlled nanocrystals and their assemblies. *J Phys Chem B* 104:1153–1175
- Gromov DG, Savitskiy AI, Pavlova LM, Borgardt NI, Grishina YS, Dubkov SV, Trifonov AY (2014) Formation of gold and silver cluster arrays using vacuum-thermal evaporation on a non-heated substrate. *Proc SPIE* 9440:94400E
- Gromov DG, Pavlova LM, Savitskiy AI, Trifonov AY (2015) Investigation of the early stages of condensation of Ag and Au on the amorphous carbon surface during thermal evaporation under vacuum. *Phys Solid State* 57:173–180
- Zimmer K, Böhme R (2008) Laser-induced backside wet etching of transparent materials with organic and metallic absorbers. *Laser Chem:170632*. <https://doi.org/10.1155/2008/170632>
- Zimmer K, Ehrhardt M, Böhme R (2010) Simulation of laser-induced backside wet etching of fused silica with hydrocarbon liquids. *J Appl Phys* 107:034908
- Sakamoto M, Fujitaka M, Majima T (2009) Light as a construction tool of metal nanoparticles: Synthesis and mechanism. *J Photochem Photobiol C Photochem Rev* 10:33–56
- Olenin AY, Lisichkin GV (2011) Metal nanoparticles in condensed media: preparation and the bulk and surface structural dynamics. *Russ Chem Rev* 80:605–630
- Kreibig U, Gartz M, Hilger A, Hövel H, Quinten M, Wagner D (2005) A short survey of optical properties of metal nanostructures. In: Kassing R et al (eds) *Functional Properties of Nanostructured Materials*. Springer, pp 75–110
- Tsvetkov MY, Bagratashvili VN, Panchenko VY, Rybaltovskiy AO, Samoilovich MI, Timofeev MA (2011) Plasmon resonances of silver nanoparticles in silica based meso-structured films. *Nanotechnol Russ* 6:619–624
- Khlebtsov NG, Dykman LA (2010) Optical properties and biomedical applications of plasmonic nanoparticles. *J. Quantitat. Spectroscopy & Radiat. Transfer* 111:1–35
- Amendola V, Polizzi S, Meneghetti M (2007) Free silver nanoparticles synthesized by laser ablation in organic solvents and their easy functionalization. *Langmuir* 23:6766–6770

31. Singh R, Soni RK (2015) Synthesis of rattle-type Ag@Al<sub>2</sub>O<sub>3</sub> nanostructure by laser-induced heating of Ag and Al nanoparticles. *Appl Phys A* 121:261–271
32. Singh R, Soni RK (2019) Laser-induced heating synthesis of hybrid nanoparticles. In: Mohapatra S, Nguyen TA, Nguyen-Tri P (eds) *Noble Metal - Metal Oxide Hybrid Nanoparticles: Fundamentals and Applications*. Elsevier, pp 195–238
33. Mock JJ, Barbic M, Smith DR, Schultz DA, Schultz S (2002) Shape effects in plasmon resonance of individual colloidal silver nanoparticles. *J Chem Phys* 116:6755–6759
34. Jin R, Cao YW, Mirkin CA, Kelly KL, Schatz GC, Zheng JG (2001) Photoinduced conversion of silver nanospheres to nanoprisms. *Science* 294:1901–1903
35. Levin I, Brandon D (1998) Metastable alumina polymorphs: crystal structures and transition sequences. *J Am Ceram Soc* 81:1995–2012
36. McHale JM, Auroux A, Perrotta AJ, Navrotsky A (1997) Surface energies and thermodynamic phase stability in nanocrystalline aluminas. *Science* 277:788–791
37. Wortmann D, Gottmann J, Brandt N, Horn-Solle H (2008) Micro- and nanostructures inside sapphire by fs-laser irradiation and selective etching. *Opt Expr* 16:1517–1522
38. Hörstmann-Jungemann M, Gottmann J, Keggenhoff M (2010) 3D-Microstructuring of sapphire using fs-laser irradiation and selective etching. *J Laser Micro/Nanoeng* 5:145–149
39. Capuano L, Pohl R, Tiggelaar RM, Berenschot JW, Gardeniers JGE, Römer GRBE (2018) Morphology of single picosecond pulse subsurface laser-induced modifications of sapphire and subsequent selective etching. *Opt Expr* 26:29283–29295
40. Lorazo P, Lewis LJ, Meunier M (2006) Thermodynamic pathways to melting, ablation, and solidification in absorbing solids under pulsed laser irradiation. *Phys Rev B* 73:134108
41. Bozhevolnyi SI, Volkov VS, Devaux E, Laluet J-Y, Ebbesen TW (2006) Channel plasmon subwavelength waveguide components including interferometers and ring resonators. *Nature* 440:508–511
42. Apuzzo A, Février M, Salas-Montiel R, Bruyant A, Chelnokov A, Léronde G, Dagens B, Blaize S (2013) Observation of near-field dipolar interactions involved in a metal nanoparticle chain waveguide. *Nano Lett* 13:1000–1006
43. Kim J (2012) Joining plasmonics with microfluidics: from convenience to inevitability. *Lab on a Chip* 19:3611–3623
44. Polavarapu L, Pérez-Juste J, Xu Q-H, Liz-Marzán LM (2014) Optical sensing of biological, chemical and ionic species through aggregation of plasmonic nanoparticles. *J Mater Chem C* 2:7460–7476

**Publisher's Note** Springer Nature remains neutral with regard to jurisdictional claims in published maps and institutional affiliations.